NASA Technical Memorandum 109141

Hypersonic, Nonequilibrium Flow over the FIRE II Forebody at 1634 sec

Lin Hartung Chambers
Langley Research Center, Hampton, Virginia

July 1994

National Aeronautics and
Space Administration
Langley Research Center
Hampton, Virginia 23681-0001

Hypersonic, Nonequilibrium Flow over the FIRE II Forebody at 1634 sec

Lin Hartung Chambers
NASA Langley Research Center
Hampton, VA 23681-0001

SUMMARY

The numerical simulation of hypersonic flow in thermochemical nonequilibrium over the forebody of the FIRE II vehicle at 1634 sec in its trajectory is described. The simulation was executed on a Cray C90 wih Program LAURA.4.0.2. The Langley Aerothermodynamic Upwind Relaxation Algorithm (LAURA) is described in References [1] and [2]. Code setup procedures and sample results, including grid refinement studies, are discussed. This simulation relates to a study of radiative heating predictions on aerobrake type vehicles.

CONFIGURATION

The configuration is an axisymmetric, truncated spherical forebody, with a small corner radius, as described in Ref. [3]. This trajectory point corresponds to the first FIRE II heatshield, with a 0.935 m nose radius.

SURFACE GRID

The surface grid surface.01 is defined with (30x1) cells. This grid was generated automatically by choosing option 2 for geometry initialization in Program Start.4.0.2. This results in grid points equally spaced along the forebody surface, with a concentration of points around the sharp corner where the flow turns into the wake. The surface grid is shown in Fig. 1. As part of the grid convergence study, a second surface grid, surface.02, of 60x1 cells was also used. This grid was generated by linear interpolation of the coarser grid.

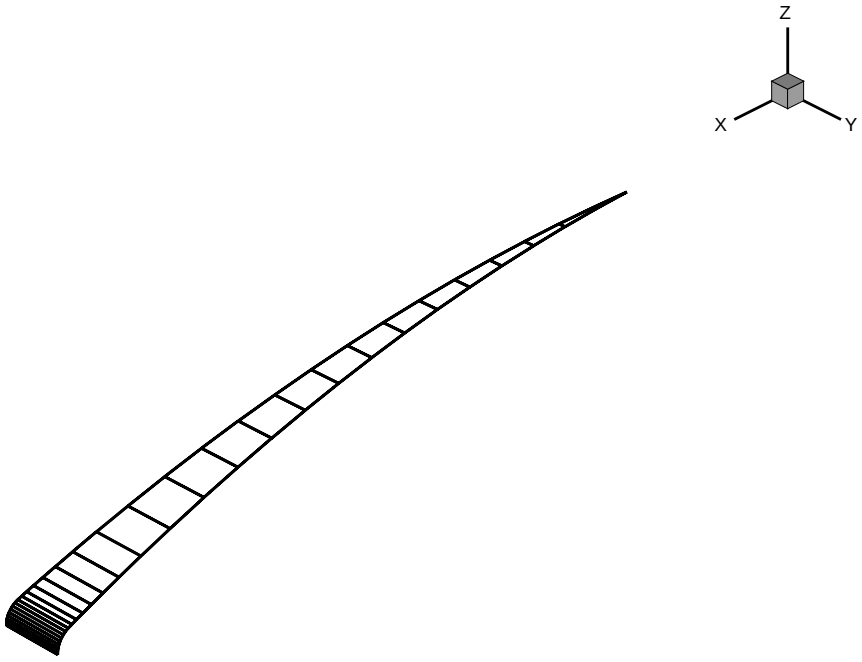

Figure 1: Baseline Surface Grid with 30 cells

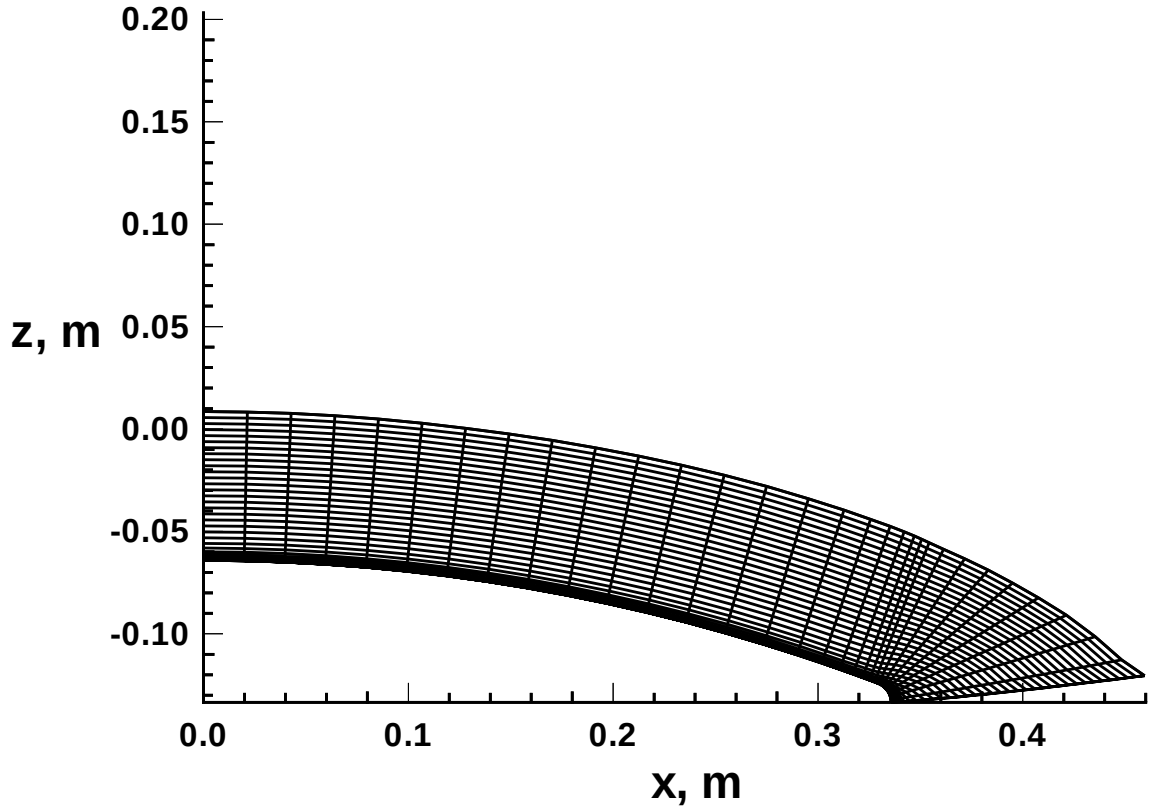

Figure 2: Baseline Volume Grid with 30 by 80 cells

VOLUME GRID

The volume grid is automatically generated and periodically adjusted within Program LAURA.4.0.2. Converged solutions were obtained with 80 cells and 128 cells across the shock layer. A global view of the 30 by 80 cell grid is shown in Fig. 2. For clarity, only every other grid line is shown in the direction normal to the body.

One baseline setting for volume grid adaption was changed for these simulations. The baseline setting in "subroutine algnshk" produces a cell Reynolds number equal to 1.0 at the wall. However, to get the flowfield to set up from a cold start this value is initially changed to 0.1 by changing the value of **recell** in file "algnshk.f" from 1.0 to 0.1. This change is made in a data statement near the beginning of the file. Once the shock layer has started to form, the cell Reynolds number is reset to 1.0.

condition	V_∞ m/s	ρ_∞, kg/m^3	T_∞, K	h, km	M_∞
01	11360.	$3.72\ 10^{-5}$	195.	76.42	40.6

Table 1: Freestream Conditions

FREESTREAM CONDITIONS

Only one set of freestream conditions was tested for this study, as shown in Table 1.

GAS MODEL

The test gas is air in thermal and chemical nonequilibrium. The laminar, thin-layer Navier-Stokes option was selected for all cases. An 11 species air model was tested, which included N, O, N_2, O_2, NO, N^+, O^+, N_2^+, O_2^+, NO^+, and e^-. The baseline gas kinetic model (**kmodel** set to 3 in file "parameter.strt") is substantially derived from the work of Park as detailed in Table 1 of Reference [4].

BOUNDARY CONDITIONS

Most of the boundary conditions were set automatically when the self start geometry option 2 (generic aerobrake) was chosen within the initialization Program Start.4.0.2. In addition, a constant wall temperature equal to 615 K and a noncatalytic (**jtype** = 0) wall option are specified during the program initialization.

NUMERICAL PARAMETERS

Standard, baseline settings for numerical parameters and options in LAURA are: eigenvalue limiter $\epsilon_0 = 0.30$ (variable **epsa** in data file) with aspect ratio scaling across the boundary layer, and symmetric limiter based on gradients of Rdq as defined in Ref. [5]. No changes to these parameters were made for any of the test cases in this report.

case number	freestream conditions	surface configuration	volume grid	gas model	boundary conditions
01	01	surface.01	80 cells	11 species	unchanged
02	01	surface.01	128 cells	11 species	unchanged
03	01	surface.02	80 cells	11 species	unchanged

Table 2: Test Matrix

TEST MATRIX

The test cases are defined in Table 2.

RUN LOGS

A record of the data file state from run to run for case 01 is included in Table 3. The variables in this table are defined in the data file. Additional parameters shown in the Table are the run number; the L2 norm at the end of the run, giving an indication of the level of convergence; and Δq_s, the change in stagnation point heating from the beginning to the end of the run, in $BTU/ft^2 - sec$. The following data file variables are kept unchanged throughout the runs: **ifrozen** = 1 (chemical source terms on), **epsa** = 0.3 (eigenvalue limiter), **errd** = 0.01 (error criterion for grid doubling).

After the self-start run with **newjob** = 2, the **newjob** parameter is set to 0 to use the output of the previous run. The grid, initially 20 cells in the **k** direction, doubled twice during run 03 to the final 80 cells. At this point the shock layer had set up sufficiently to return **recell** to its normal value for run 04. In run 05 two grid alignments were performed to redistribute the grid based on **recell** and the developing shock layer. For runs 06 through 09, the values of **itervmx** and **niterp** were gradually increased. These control the number of iterations between transport property and Jacobian updates, respectively. As the solution becomes established, larger values are acceptable.

From this point, the remaining runs are to obtain convergence in the stagnation point heating rate. The change in stagnation point heating rate is recorded in the last column for those runs in which it was monitored. The shock was aligned twice more in run 10 and again in run 22 to obtain fine adjustments in the boundary layer. At the end of run 13, the solution exhibited some signs of instability, so the inviscid and viscous relaxation factors, **rfinv** and **rfvis**, were adjusted slightly.

The error norm, denoted **L2 norm**, dropped nicely through run 09, with upward spikes for grid doubling and shock alignments. Fig. 3 shows the error norm as a function of iteration number for the complete solution. Around run 11 the error norm began an upward trend, and the figure indicates the solution may be on the edge of stability. To enhance the convergence, as mentioned above, **rfinv** and **rfvis** were adjusted and the behavior of the error norm improved.

With the full 30 by 80 cell grid, the C-90 computes approximately 3 iterations per second. The complete solution therefore required about 3 hours of Cray C-90 time.

The change in stagnation point heating between runs 28 and 29 was less than 0.2%, and the solution is therefore considered converged.

run	newjob	nord	itervmx	niterp	iterg	movegrd	rfinv	rfvis	recell	L2 norm	Δq_s
01	2	1	1	1	100	0	2.00	1.00	0.1	7.048e-2	
02	0	1	1	1	100	0	2.00	1.00	0.1	1.518e-2	
03	0	1	1	1	200	0	2.00	1.00	0.1	1.597e-1	
04	0	1	1	1	200	0	2.00	1.00	1.0	6.011e-3	
05	0	1	1	1	200	100	2.00	1.00	1.0	3.222e-2	
06	0	2	2	2	200	0	2.00	1.00	1.0	1.21e-2	
07	0	2	5	5	500	0	2.00	1.00	1.0	1.832e-3	
08 - 09	0	2	10	10	1000	0	2.00	1.00	1.0	1.123e-4	+16
10	0	2	10	10	100	40	2.00	1.00	1.0	7.67e-3	
11	0	2	10	10	1000	0	2.00	1.00	1.0	5.786e-5	+8
12 - 13	0	2	20	20	1780	0	2.00	1.00	1.0	6.348e-5	+18
14	0	2	10	10	1650	0	2.10	1.10	1.0	1.577e-5	+6
15	0	2	10	10	2000	0	2.10	1.10	1.0	1.014e-5	+6
16 - 18	0	2	10	10	1650	0	2.10	1.10	1.0	3.255e-6	+11.5
19 - 21	0	2	10	10	1660	0	1.80	0.80	1.0	1.254e-6	+7.6
22	0	2	10	10	15	10	2.00	1.00	1.0		
23 - 26	0	2	10	10	1650	0	2.00	1.00	1.0	7.508e-5	+3
27 - 29	0	2	10	10	1650	0	3.00	1.00	1.0	3.109e-8	+0.9
30	0	2	10	10	200	0	3.00	1.00	1.0	2.973e-8	

Table 3: Data File and Convergence Log - Case 01

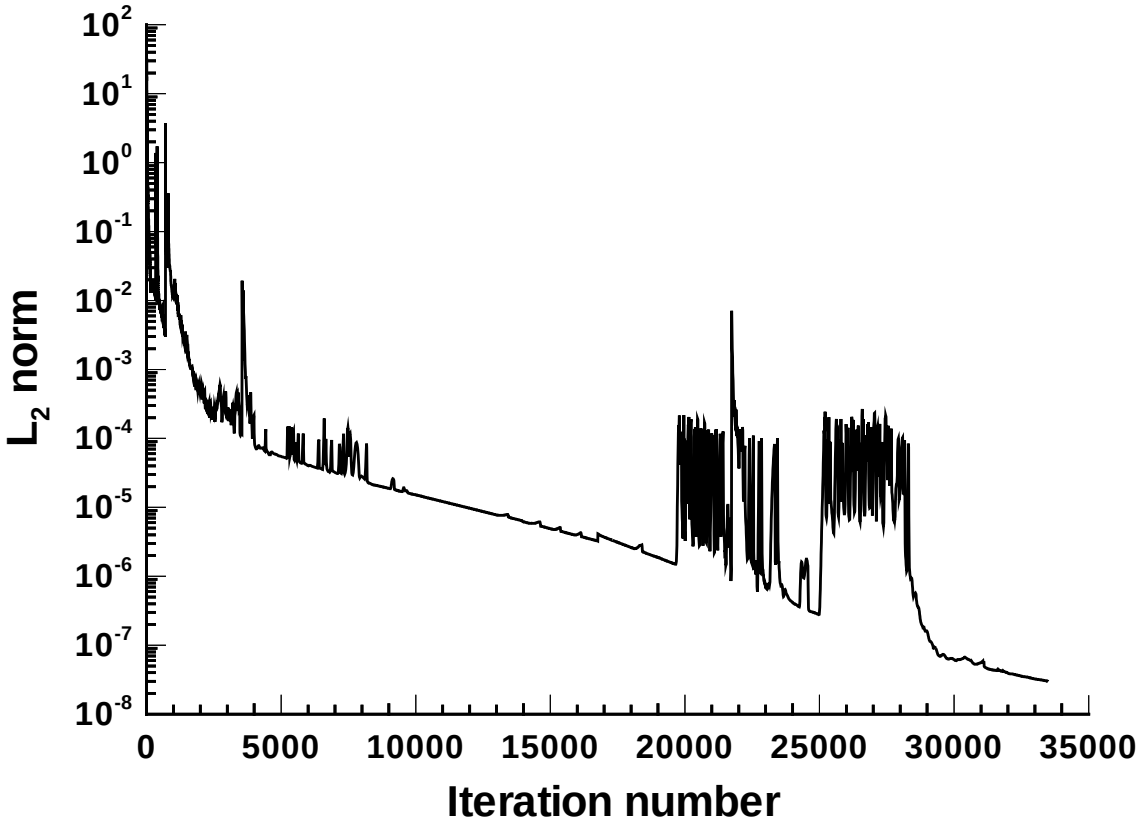

Figure 3: Convergence history for Case 01

run	newjob	nord	itervmx	niterp	iterg	movegrd	rfinv	rfvis	recell	L2 norm	Δq_s
31	0	2	10	10	200	50	3.00	1.00	1.0	4.749e-4	
32	0	2	10	10	1020	0	3.00	1.00	1.0	1.203e-5	+1.5
33	0	2	10	10	1040	0	3.00	1.00	1.0	3.238e-7	+0.5
34	0	2	10	10	1040	0	3.00	1.00	1.0	3.108e-8	+0.4
35	0	2	10	10	1040	0	3.00	1.00	1.0	6.323e-8	+0.2
36	0	2	10	10	1040	0	3.00	1.00	1.0	5.293e-8	+0.2

Table 4: Data File and Convergence Log - Case 02

run	newjob	nord	itervmx	niterp	iterg	movegrd	rfinv	rfvis	recell	L2 norm	Δq_s
31	0	2	10	10	1000	0	3.00	1.00	1.0	1.985e-7	+0.2
32	0	2	10	10	1000	0	3.00	1.00	1.0	8.344e-8	+0.1
33	0	2	10	10	1000	0	2.00	1.00	1.0	3.309e-8	

Table 5: Data File and Convergence Log - Case 03

Run logs for cases 02 and 03, starting from the converged solution of case 01, are given in Tables 4 and 5. Case 02 was started by rerunning PRELUDE with the appropriate grid size, and selecting **newjob** = 0, to start with the converged restart file from Case 01. Case 03 was started by applying a restart file processing program developed to double the grid in the **i** direction. This program basically interpolated the Case 01 solution and wrote a new restart file with twice the grid cells in the **i** direction.

For Case 02, grid adjustment was turned on for the first run (denoted run 31 because this case started from the converged Case 01). This allowed the grid to increase from 80 to 128 cells in the normal direction, and to readjust the distribution accordingly. After that, **movegrd** was set to 0 and the stagnation point heating was converged, again to a level of less than 0.2% change. The convergence history for this case is shown in Fig. 4. Initially the error norm takes a large jump, as the grid is readjusted. It then converges rapidly to a low level where it finally stalls out.

For Case 03, grid adjustment in the **k** direction is not necessary, so just three runs were required to converge the stagnation point heat flux with the change to 60 by 80 cells. In this case it was converged to less than 0.1%. The error norm for this case is quite boring, decreasing monotonically to the order of 10^{-8} very quickly after the initial disturbance.

RESULTS

The effect of the various grid distributions on convective heating is shown in Figure 5. Differences in heating are less than 1 percent at any point on the body. The baseline Case 01 solution can therefore be considered grid converged.

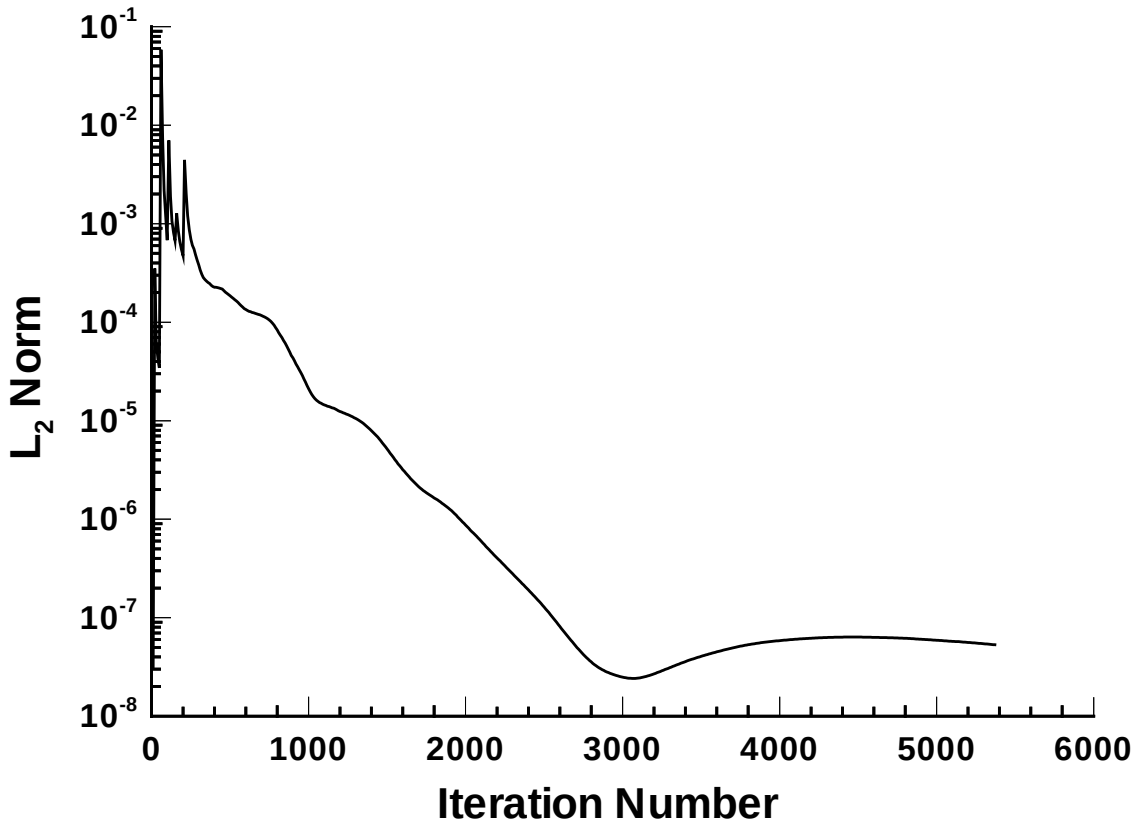

Figure 4: Convergence history for Case 02

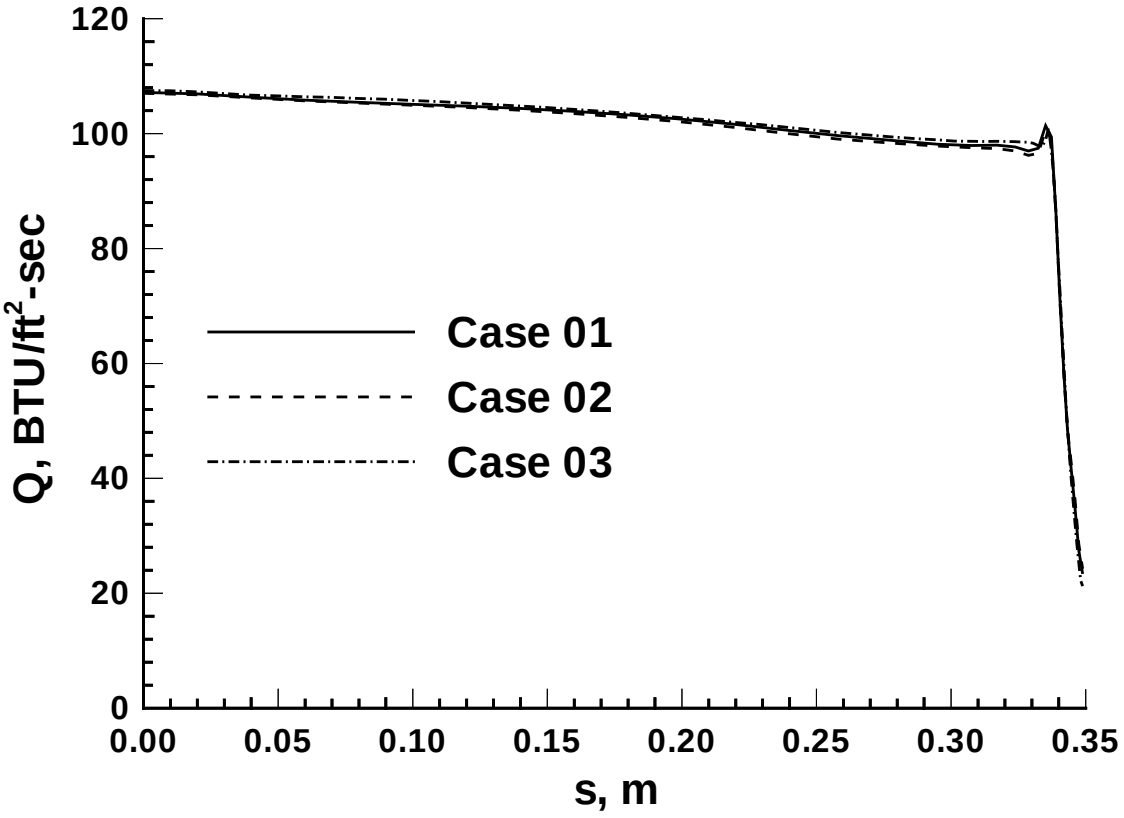

Figure 5: Convective Heating for Cases 01, 02, and 03

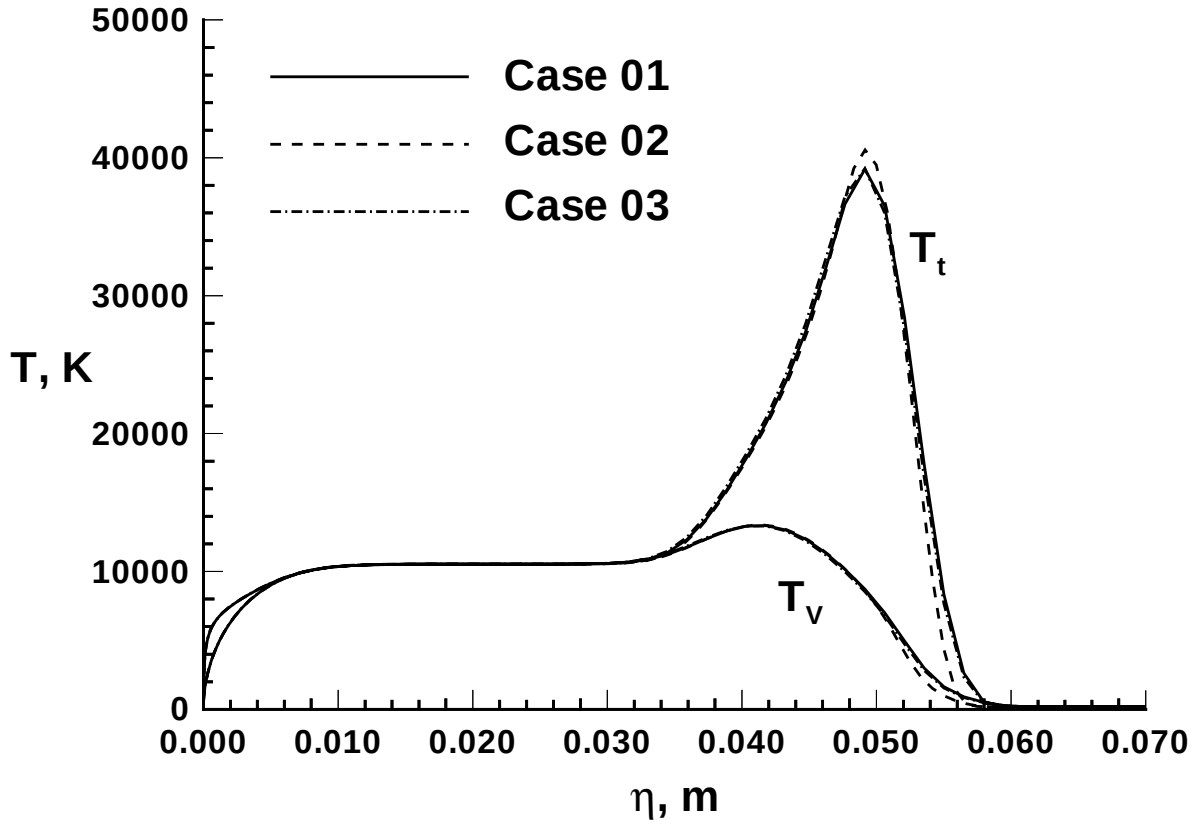

Figure 6: Shock Layer Temperature Profiles for Cases 01, 02, and 03

Shock layer profiles taken from cell centers adjacent to the stagnation streamline are presented for cases 01 - 03 in Figure 6. The cell centers for cases 01 and 02 are offset approximately 2 cm from the stagnation streamline and cell centers from case 03 are offset approximately half as much. The effect of the finer grid in Case 02 is to slightly improve the solution in the captured shock. This effect appears in other variables as well, but as shown above has no effect on convective heating.

To further examine this solution, the LORAN radiation prediction method of Ref. [6] was applied to Case 01 and Case 02. This method provides radiative flux distributions along the FIRE II vehicle surface and in the shock layer. As shown in Figure 7, the radiative flux to the surface is more sensitive than the convective flux to the resolution of the shock front, with a maximum variation of 3 percent occurring at $s \approx 12\ cm$. The reason for this can be seen in Figure 8, where the variation of flux toward the wall through the shock layer is displayed as a function of the normal coordinate, η (the top curve is from the cell centers adjacent to the stagnation line, the lower curve is along a surface normal near the shoulder). This property is quite sensitive to the small changes in temperature in the captured shock. As a result, minor variations in alignment of the grid with respect to the shock can cause the q_R variations shown in Fig. 7.

While the radiative flux result also suggests a grid-converged solution, looking more closely at the radiation result may bring this conclusion into question. Figure 9 shows the divergence of the

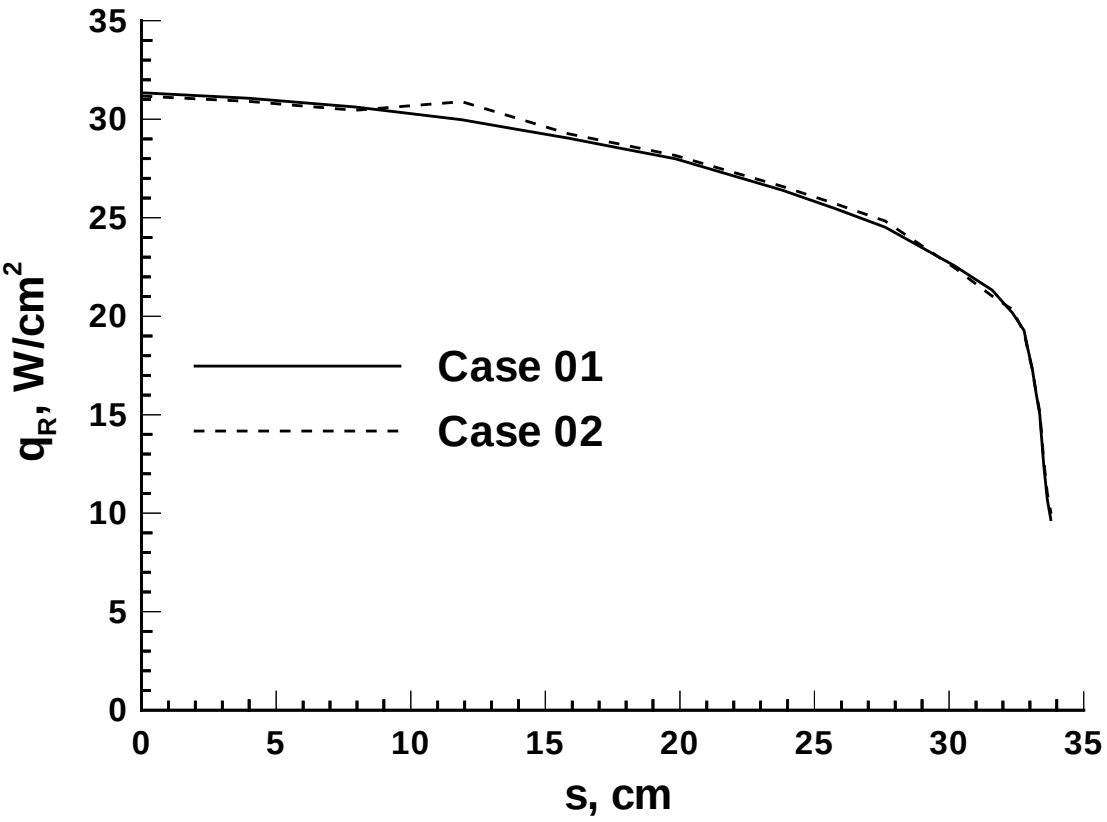

Figure 7: Wall Radiative Heat Flux for Cases 01 and 02

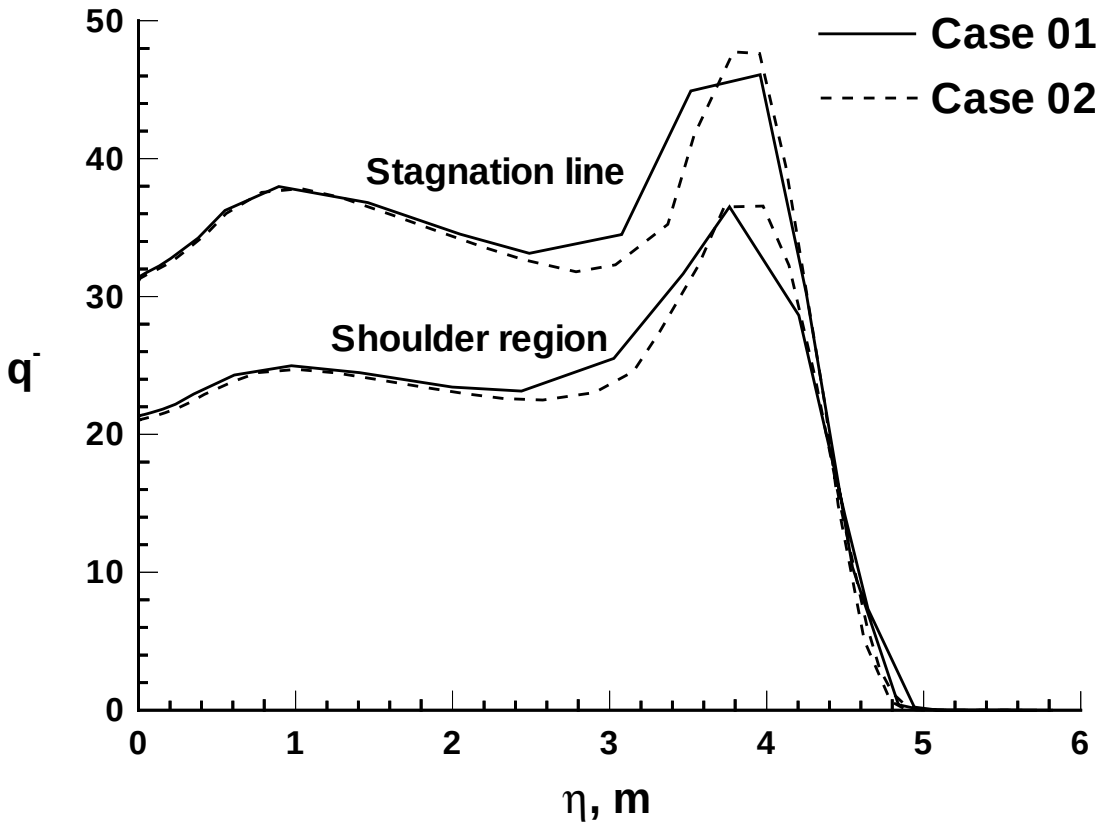

Figure 8: Wall-Directed Radiative Flux Profiles for Cases 01 and 02

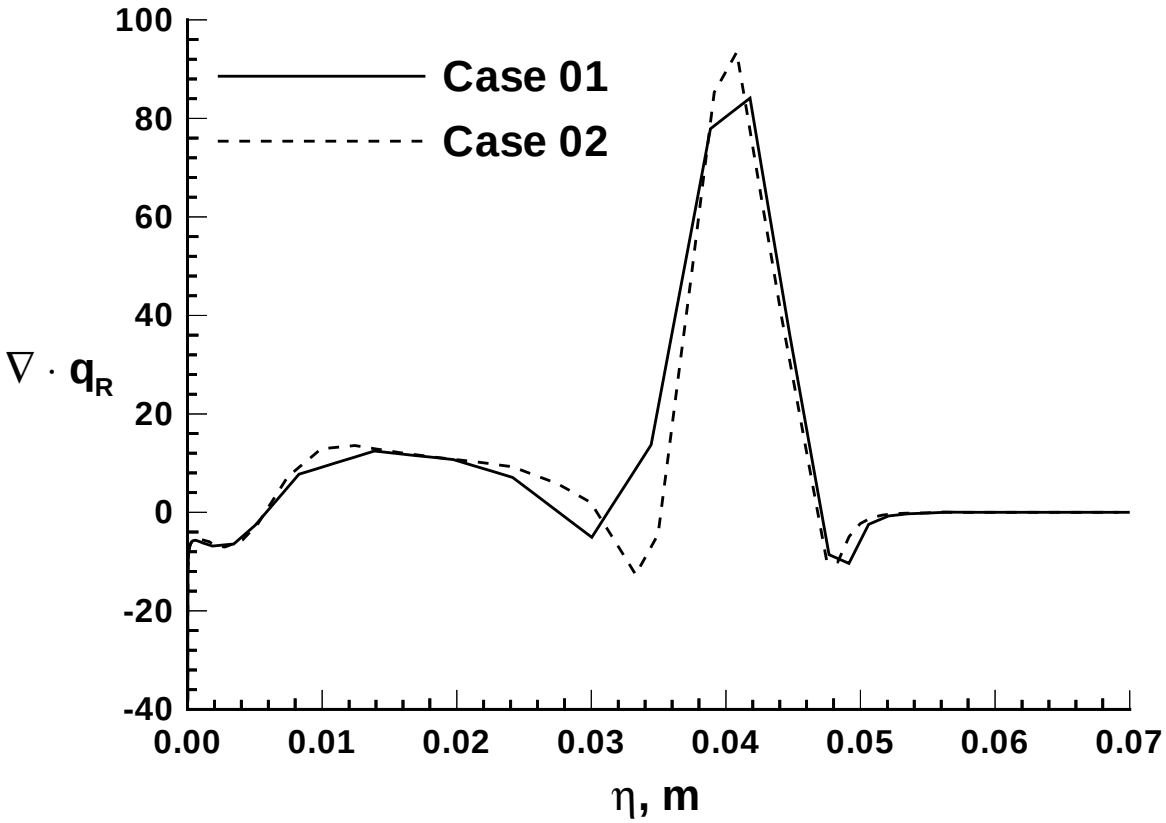

Figure 9: Divergence of the Radiative Flux for Cases 01 and 02

radiative flux along the cell centers next to the stagnation line. This is the quantity which appears in the energy equation to couple the fluid flow and the radiative transport. The curves suggest that the details of this coupling may be quite different for Case 01 and Case 02. As a result, grid convergence for radiatively coupled solutions may require extra care.

CONCLUSIONS

A hypersonic, nonequilibrium solution has been obtained with the LAURA flowfield code. Details of the solution convergence procedure are presented to aid a novice user of the code. The heating results presented here may be considered grid converged unless coupled radiation is required in the solution. Maximum differences in convective heating are below 1 percent, and below 3 percent in radiative heating.

REFERENCES

[1] P. A. Gnoffo, R. N. Gupta, and J. L. Shinn, "Conservation Equations and Physical Models for Hypersonic Air Flows in Thermal and Chemical Nonequilibrium," NASA TP 2867, February 1989.

[2] P. A. Gnoffo, "Point-Implicit Relaxation Strategies for Viscous, Hypersonic Flows," in *Computational Methods in Hypersonic Aerodynamics* (T. Murthy, ed.), pp. 115–151, Computational Mechanics Publications, Kluwer Academic Publishers, 1991.

[3] D. L. Cauchon, "Radiative Heating Results from the FIRE II Flight Experiment at a Reentry Velocity of 11.4 Kilometers per Second," NASA TM X-1402, July 1967.

[4] C. Park, J. T. Howe, R. L. Jaffe, and G. V. Candler, "Chemical-Kinetic Problems of Future NASA Missions," AIAA Paper 91-0464, January 1991.

[5] K. J. Weilmuenster and P. A. Gnoffo, "Solution Strategies and Heat Transfer Calculations for Three-Dimensional Configurations at Hypersonic Speeds," AIAA Paper 92-2921, July 1992.

[6] L. C. Hartung, "Development of a Nonequilibrium Radiative Heating Prediction Method for Coupled Flowfield Solutions," *Journal of Thermophysics and Heat Transfer*, vol. 6, pp. 618–625, Oct.-Dec. 1992.

APPENDIX A - INPUTS file for initialization

```
  8 .........................................number of processors
  2 .........geometry:  0=externally generated, 1=conic, 2=aerobrake
  1 ............................flow:  1=axisymmetric, 2=2-D, 3=3-D
  1 ..........................fluid eqns:  0=inviscid, 1=TSL, 2=N-S
  10360.0     ..................................................velocity [m/s]
 0.372000E-04 ................................................density [kg/m^3]
  195.000     ....................................freestream temperature [K]
  0 .........Tw bc:  0=constant, 1=variable, 2=equilibrium radiative
  615.000     ..........................................wall temperature [K]
  2 ................................gas model:  0=PG, 1=EQ, 2=NONEQ
  2 .....thermal state:  1=equilibrium (1-T), 2=nonequilibrium (2-T)
y ............................species:  atomic nitrogen (y/n)?....
y ............................species:  atomic oxygen.............
y ............................species:  molecular nitrogen........
y ............................species:  molecular oxygen..........
y ............................species:  nitric oxide..............
y ............................species:  ionized atomic nitrogen...
y ............................species:  atomic oxygen.............
y ............................species:  ionized molecular nitrogen
y ............................species:  ionized molecular oxygen..
y ............................species:  ionized nitric oxide......
  0 ................................catalytic nature of wall (jtype)
 30 ............................cells in streamwise/axial direction
 80 ............................cells in normal direction (maximum)
  2 ...........aerobrake geometry option:  0=AFE, 1=sphere, 2=custom
  0 ...................................units:  0=m, 1=cm, 2=ft, 3=in
  69.3638     ..........................................body half angle [deg]
  69.3638     ....................................shoulder turning angle [deg]
 0.100000E-01 ..........................................shoulder radius [m ]
 0.935000     ..............................................nose radius [m ]
 0.336000     ..........................................base plane radius [m ]
```